



Of fractal and Fourier: A measure for local shape complexity for neurological applications

Erin I. Walsh*, Tianqi Zhang, Nicolas Cherbuin

Centre for Research on Ageing, Health and Wellbeing, The Australian National University, Canberra, Australia

ARTICLE INFO

Keywords:

Local shape complexity
Fractal dimensionality
Elliptical Fourier

ABSTRACT

Background: Local shape complexity can be biologically meaningful as a marker of disease, trauma, or change in brain structure over time. Fractal dimensionality (FD) is currently the dominant measure of local shape complexity used in neuroimaging but its limitations are not well understood.

New method: Elliptical Fourier harmonic power requirement (HPR) may provide complementary information to FD. We benchmarked the performance of FD and HPR on a series of simulated shapes, systematically manipulating aspects of local shape complexity, and a series of clinical contours (glioma tumour cores and stroke lesions from the BRATS and ATLAS datasets). HPR was calculated at the point of 99.9% harmonic power. FD was calculated at six resolutions (8×8 , 16×16 , 32×32 , 64×64 , 128×128 , and 256×256), by using an approach which computationally indexes the complexity of the shape boundary (i.e. the number of cells defining the contour) relative to the total grid size.

Results and comparison with existing methods: PR and FD were moderately positively correlated ($r \approx 0.2$ to 0.8 depending on shape properties), and both were sensitive to the frequency and amplitude of local complexity. FD was most biased by rotation, while HPR was more biased by global shape features such as deep invaginations. FD indicated an aggregate measure of complexity across the whole contour, while HPR indicated the point of highest complexity.

Conclusions: The HPR index provides conceptually distinct local complexity information from the current FD standard. Future research will benefit from using these complementary measures.

1. Introduction

Local shape complexity in structural neuroimaging shows promise in differentiating healthy from pathological brain development, ageing, and disease, particularly when gross morphological characteristics are insensitive or unclear (Di Ieva et al., 2015; Madan and Kensinger, 2017). The most commonly used measure, fractal dimensionality (FD), deconstructs shapes into grids of varying dimensions (Di Ieva et al., 2015, 2014; Madan and Kensinger, 2017). The grid cells (“boxes”) denoting the outer contour are counted, and the relationship between box count and grid size indicates shape complexity: as box size decreases, box count increases, so the steeper the slope of this association, the greater the complexity (Di Ieva et al., 2014). While this approach has proven useful in neuroimaging, particularly for quantifying age-associated cortical and subcortical changes in brain structure and as a surrogate biomarker for brain damage and neurological alterations in disease (Di Ieva et al., 2015), it has yet to be benchmarked across

different forms of local complexity, such as puckering (as may be incurred during cancer tumour growth), or randomly distributed ragged lesions (as may be observed in lesions following stroke).

We propose an alternative method for exploring shape complexity. Elliptical Fourier (eFourier) has been applied in the neuroimaging literature to examine global shape (Ferrario et al., 1994). eFourier techniques deconstruct shape into a series of overlapping trigonometric harmonics which deform an ellipse, where low amplitude harmonics (fit first) capture lower frequency shape characteristics, while higher amplitude harmonics (fit later) capture higher frequency shape characteristics (Caple et al., 2017; Kuhl and Giardina, 1982). Local complexity is high frequency information, so higher amplitude harmonics capture local shape information after global shape has been established by lower amplitude harmonics. It follows that the point where optimal shape fit is reached (denoted by 99.9% harmonic power) is a possible index of local shape complexity. The concept of harmonic power is not new, as it is widely used to calibrate the number of harmonics required

* Corresponding author at: Centre for Research on Ageing, Health and Wellbeing, Centre for Research on Ageing, Health and Wellbeing, 54 Mills Road, Australian National University, Acton, ACT, 2601, Australia.

E-mail addresses: erin.walsh@anu.edu.au (E.I. Walsh), tianqi.zhang@anu.edu.au (T. Zhang), nicolas.cherbuin@anu.edu.au (N. Cherbuin).

<https://doi.org/10.1016/j.jneumeth.2019.05.009>

Received 5 September 2018; Received in revised form 19 May 2019; Accepted 20 May 2019

Available online 21 May 2019

0165-0270/© 2019 Published by Elsevier B.V.

in Fourier analysis. Our approach of using it explicitly as a measure of local complexity is novel. We call this the Harmonic Power Requirement (HPR).

These methods are most distinct in whether they reflect average complexity over an entire contour (as in FD, which is calibrated against the total box count of the whole contour), or only the most complex part (as in HPR, which is calibrated against the highest frequency required anywhere on a contour). This is meaningful in circumstances when only a sub-section of a topical neural shape may exhibit local complexity. Accordingly, benchmarking and comparison of both methods will clarify their sensitivity, specificity and comparative properties for measuring local shape complexity.

2. Materials and methods

All work was undertaken in R version 3.2.0 using original code, and the *rgeos* (version 0.3.15), *shapes* (version 1.1.11), and *sp* (version 1.2–3) packages.

2.1. Measures of local complexity

The methods for ascertaining local complexity are summarized visually in Fig. 1. Elliptical Fourier analysis of contours and calibration to detect the point of 99.9% harmonic power was undertaken in the *Momocs* package (version 0.9.48), as described in Bonhomme et al. (2014). Briefly, as outlined in Kuhl and Giardina (1982), elliptical Fourier analysis comprises deformation of an ellipse via pairs of harmonics for the x (A_n , B_n) and y (C_n , D_n) axes. As shown in Fig. 1 (panel A), each additional harmonic ($A_1/B_1/C_1/D_1$, $A_2/B_2/C_2/D_2$... $A_{10}/B_{10}/C_{10}/D_{10}$, etc) increases the detail captured, as higher frequency harmonics capture higher frequency shape features such as corners. The utility of additional harmonics is subject to diminishing returns that is a function unique to each shape (Fig. 1, panel C), thus harmonic power is typically used to ascertain the point at which additional harmonics do not improve shape fidelity. Harmonic power at any given n as $\frac{A_n^2 + B_n^2 + C_n^2 + D_n^2}{2}$. This formula is applied in a cumulative sum for 1- n harmonic series until 99% power is reached. Classically, this is interpreted as sufficient harmonic power for later global shape analysis with the number of harmonics being of little theoretical interest; the current interpretation re-contextualizes this existing metric as a meaningful index of local complexity.

For FD, the *raster* (version 2.4.20) and *sp* (version 1.2-1) packages were used to decompose shapes into varying grid sizes (e.g. Fig. 1 panel A) based on typical MRI resolutions for subcortical structures (8×8 , 16×16 , 32×32 , 64×64 , 128×128 , and 256×256). Unlike HPR, fractal dimensionality is a linear association between grid size and number of boxes denoting the shape's contour on that grid (Fig. 1 panel C), calculated as in Madan and Kensinger (2017),

$$FD = - \frac{\Delta \log_2(\text{border count})}{\Delta \log_2(\text{grid size})}$$

The resolution of FD is bounded by the grid provided, and it naturally ranges between 1 and 2 (an artefact of referring to two-dimensional contours). The resolution of HPR is bounded by the number of points denoting the contour (as one needs twice as many points as harmonics in order to fit an eFourier curve, again reflecting the two-dimensional nature of the contours). HPR has a lower bound of 1 (which will always be an unmodified ellipse), and theoretically no upper bound: with an arbitrary number of points there can be an arbitrary number of harmonics. To our knowledge there has been no benchmarking of HPR to establish rigorous expectations of where 99.9% harmonic power is likely to be reached, but in practise there is limited meaningful detail in most contours, and so it is most common to use comparatively few (between 10 and 24 harmonics). Accordingly, we have imposed an upper bound of 100 harmonics, thus a theoretical

maximum HPR of 100, but expect substantially lower values.

As the purpose of the current paper is the relative performance of FD and HPR within a constrained set of shapes (rather than the establishment of norms), for clarity of comparison, HPR and FD were scaled into z scores relative to the mean and standard deviation of the entire simulated population for each set of simulations to create indices which fall between 0 (no local complexity) to 1 (extreme local complexity). In this way, a smooth circle has a value of 0 for both indices.

2.2. Simulated shapes

While FD has been used capture complexity in a large number of publications, to our knowledge, there is no extant set of shapes with precisely known degrees of local complexity against which FD or HPR may be benchmarked. Accordingly, the only option available is to generate shapes with induced complexity which systematically varies in magnitude in a known manner.

Shape simulation and manipulation are summarized in and Fig. 2, and explained in depth in the supplementary materials. We began with eleven two-dimensional non-self-intersecting contours denoted by 50 pairs of xy coordinates (3–13 sides, one complex; Fig. 2 panel A). We then induced three forms of local complexity depicted in Fig. 2 panel B: random (where each point denoting the contour was moved completely at random); recursive (inducing recursive triangular fractal-like complexity); and regular (where every second point was contracted), $n = 33$.

The degree of local complexity present can be thought of two elements; the amplitude and the frequency. Amplitude is the distance points may be offset in random complexity, the number of iterations in recursive complexity, and the depth of the offset in regular complexity. Five versions of amplitude, from shallow to deep, were manipulated for each of the local complexity forms of each of the 11 base shapes, resulting in 165 shapes varying in local complexity amplitude (see Fig. 2 panel C and supplementary Fig. 2). Frequency is the distance between points in random and regular complexity, and the number of triangles per edge in recursive complexity. Five versions of frequencies, from widely spaced to narrowly spaced, were manipulated for each of the local complexity forms of each of the 11 base shapes, and then matched on amplitude, resulting in 150 shapes varying in local complexity frequency (see Fig. 2 panel D and supplementary Fig. 3).

Shape is the aspect of form that is invariant across rotation, re-scaling, and translation¹. Rotation is a non-shape property common in neuroimaging, therefore a successful measure of local complexity should be insensitive to rotation. All shapes were rotated through 360 degrees. Each of the three forms of local complexity was induced in each of the 11 base contours (33 contours), resulting in each of the local complexity forms of each of the 11 base shapes, and then matched on amplitude, resulting in 11,880 shapes varying in rotation (see Fig. 2 panel E, supplementary figure 4).

There are many circumstances where only a sub-section of a contour may have local complexity, such as where a lesion or physical injury impacts on only one end of a given contour (e.g. one end of the corpus callosum, one corner of the hippocampus). Accordingly, we manipulated percentage of complexity: each contour was spliced with local complexity of each of the three forms, such that the final contour had varying percentages of local complexity (0%, 10%, 20%, ...100%; $n = 363$; Fig. 2 panel F, supplementary figure 5).

2.3. Real shapes

Real-world biological contours were selected to contrast FD and HPR performance in terms of scale and complexity; tumor growths are

¹ Small CG. *The statistical theory of shape*. Springer Science & Business Media; 2012.

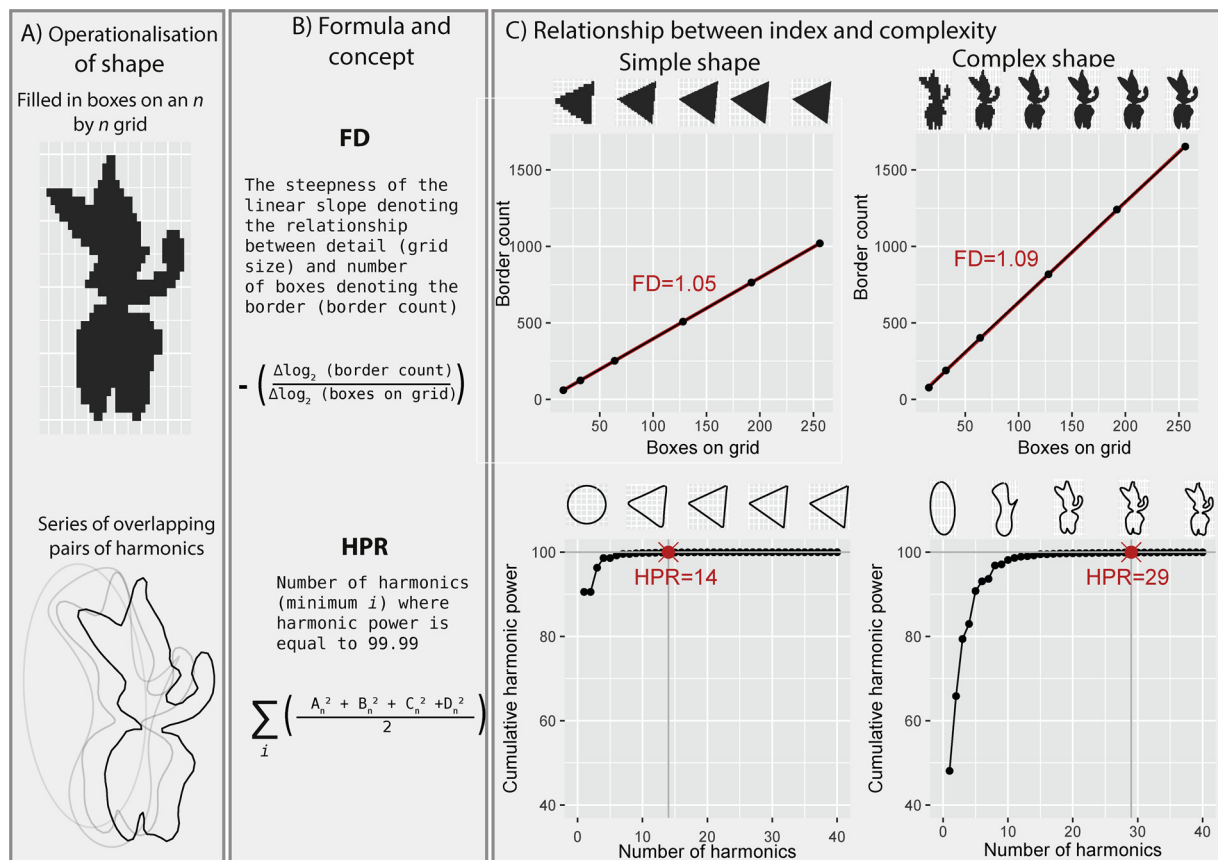


Fig. 1. Conceptual and applied process of extracting HPR and FD.

This figure summarises how Fractal Dimensionality (FD) and Harmonic Power Requirement (HPR) conceptualise local complexity. Panel A: FD operationalises shape in terms of boxes on a grid. Here, local complexity is the slope denoting the linear relationship between the size of boxes on the grid, and how many are filled by that shape. HPR operationalises shape in terms of overlapping harmonics which deform an ellipse, with higher harmonics providing higher frequency detail. Panel B summarises the logic and formulae. Panel C: The relationship between additional harmonics and improvement of shape operationalisation is non-linear in a way that is unique to each shape, but there is always a point at which adding more harmonics does not improve the fit of the shape. Here, the measure of local complexity is the cumulative sum of the harmonics required to reach this point, 99.9% harmonic power.

comparatively larger and smoother, while stroke lesions are comparatively smaller and more jagged in shape. Glioma tumour cores were obtained from The Multimodal Brain Tumour Image Segmentation Benchmark (BRATS) challenge (Bakas et al., 2017; Menze et al., 2015). Briefly, this is a collection of 65 multi-contrast MR scans of low- and high-grade glioma patients, taken at 1.5–3 T across several scanners and resampled images to 1 mm isotropic resolution in a standardized axial orientation. For the current study, we focus on the BRATs manual segmentation of the “gross core” of the tumour; the necrotic, cystic and enhancing substructure (but not surrounding oedema) undertaken on T1 scans. Lesions following stroke were obtained from the Anatomical Tracings of Lesions After Stroke (ATLAS) Dataset - Release 1.1 (Liew et al., 2017). Briefly, this open source data collection consists manual tracings of post-stroke lesions from 304 T1-weighted 1.5–3 Tesla anatomical MRI images collected from research groups in the ENIGMA Stroke Recovery Working Group consortium. In the current study, we converted tumour cores and stroke lesions from participant native space into two-dimensional contour (xy coordinates) in R, taking the slice along the anterior-posterior axis with the largest volume (thus maximising the size of the contours). This resulted in a final set of 285 tumour and 487 lesion shapes (as some individuals had multiple tumours or strokes). More information regarding this process can be found in supplementary figure 6.

2.4. Statistical analysis

For simulated shapes, a series of general linear models were fit, with

each local complexity manipulation (form, amplitude, frequency, rotation, and percentage) as a predictor of HPR or FD. Sensitivity to local shape properties (amplitude and frequency) will be manifest in a positive association between the known degree of local shape properties and the indices. Specificity to local shape will be manifest in the comparative strength of associations between local shape manipulations and the index, and the associations between global (number of sides) or non-shape (rotation) manipulations and the index. Specificity to how much of the contour exhibits local complexity will be manifest in the association between the percentage of the contour with local complexity, and the index. For clinical contours (glioma cores and stroke lesions), the measures were compared in terms of correlation and range. In order to ascertain whether HPR may provide information beyond FD (and thus be useful), correlations between HPR and FD were used to ascertain whether they are measuring the same (high correlation) or different (low correlation) local complexity features.

3. Results

3.1. Simulated shapes

Simulated shape results are summarised in Fig. 2, Table 1, and supplementary materials. HPR and FD were moderately positively correlated ($r \approx 0.2$), and both indices increased with amplitude, frequency, and percentage (Table 1), indicating both indices are sensitive to local complexity but focus on different features. FD was more sensitive to recursive and random local complexity, while HPR was most

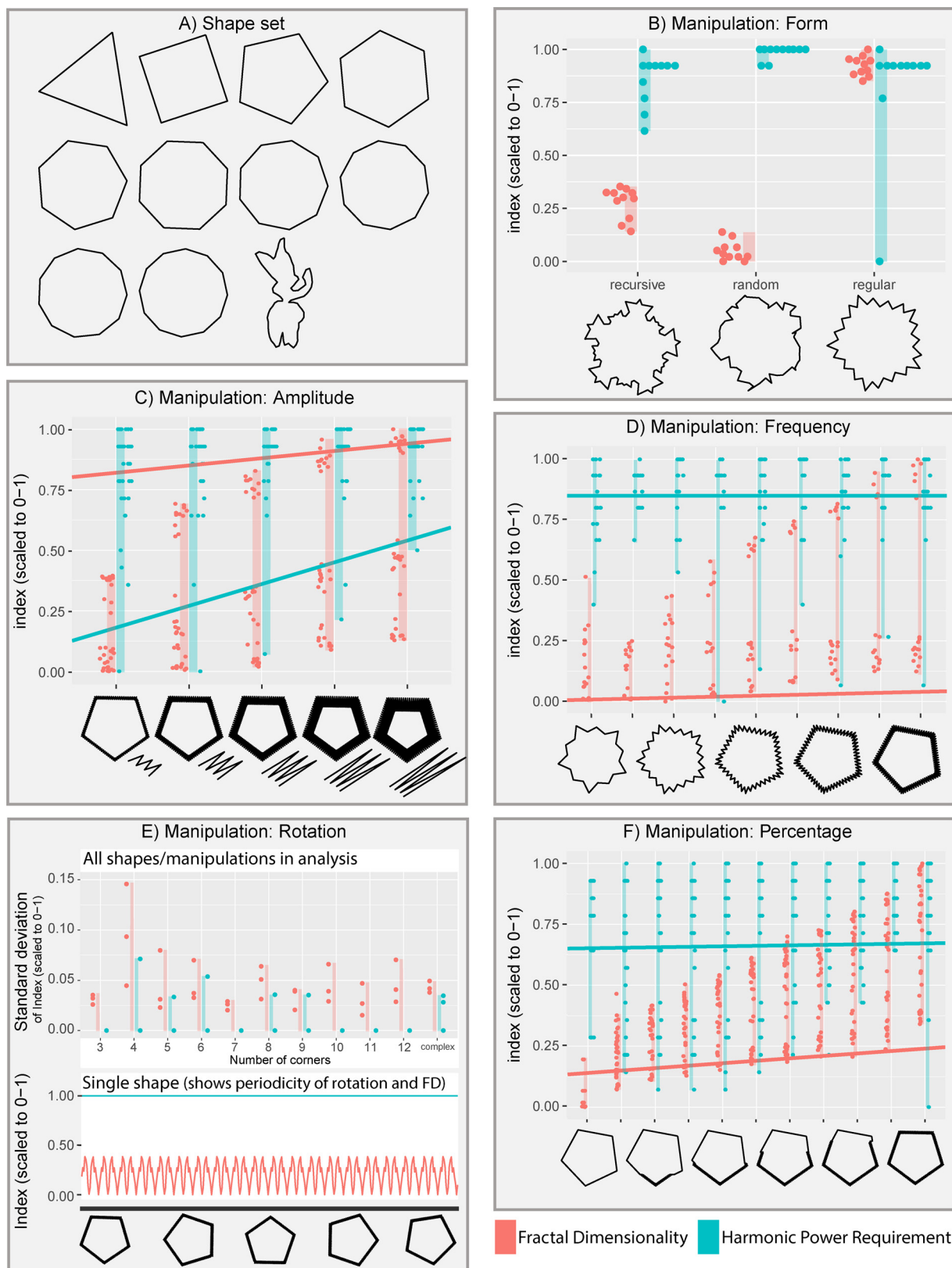


Fig. 2. Simulated Results.

Panel A: The “shape set” panel demonstrates the selected eleven contours to be manipulated; 3 through 12 corners, and one complex contour. Remaining panels B through F summarise results over each manipulation. The x-axis denotes the degree of manipulation, shown by example 5-cornered contour (where points denote values for all eleven contours). These demonstrate the range, as fewer shapes than manipulations have been selected for clarity (e.g. there were 365 rotations, but only five are shown). The y-axis provides either FD (red) or HPR (blue) index for a given contour (point) and the range across contours (boxes). For all but ‘form’ and ‘rotation’, these summaries include all three forms of local complexity (recursive, random, and regular), thus plots C through F have 33 possible points (hence minor jittering to avoid overplotting). In panel E, the points denote the standard deviation of FD and HPR indices across 360 degrees of rotation, with one point per form of complexity. Similar plots deconstructed across these three forms of local complexity can be seen in the supplementary materials.

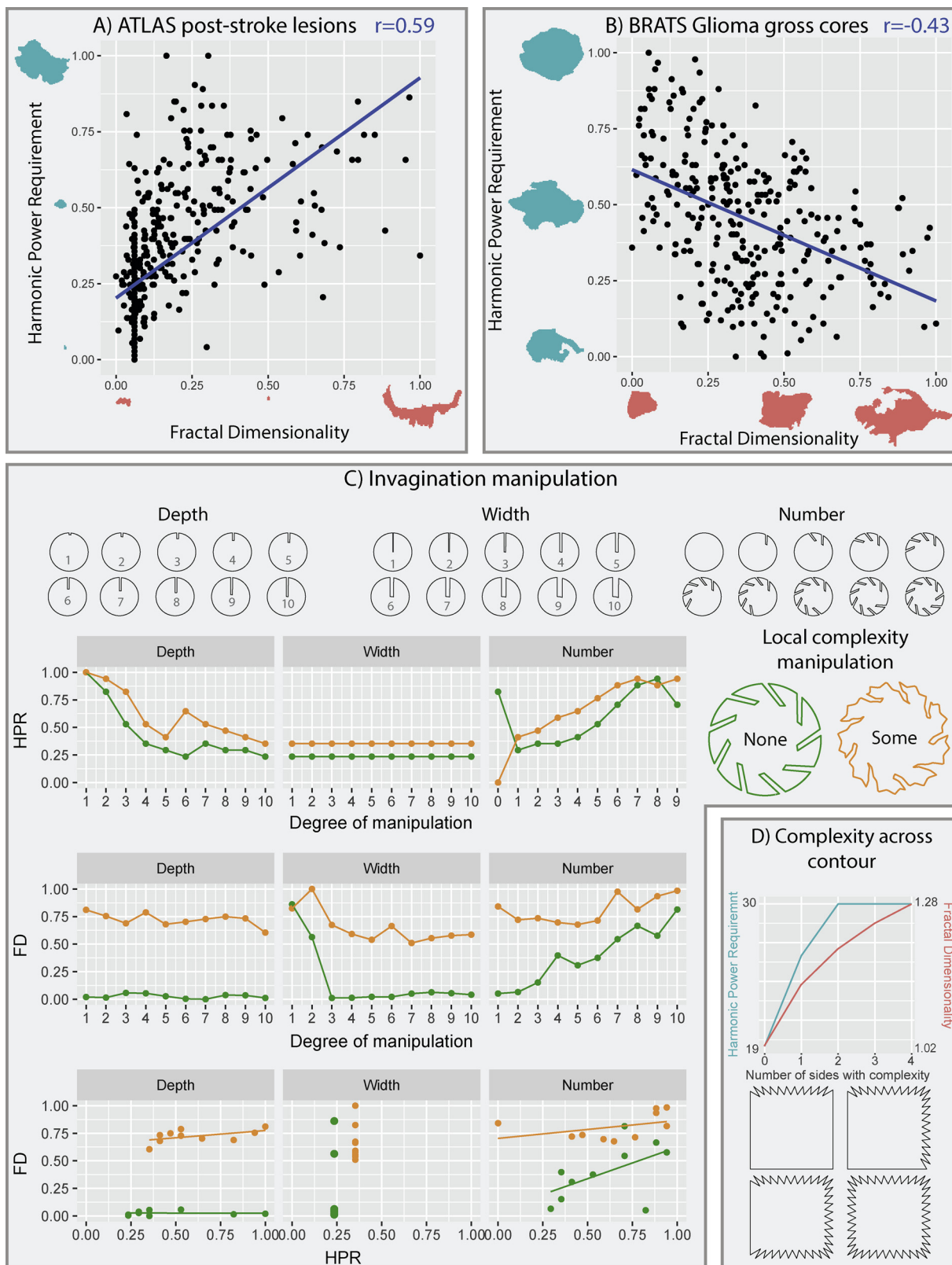


Fig. 3. Real Contour and post-hoc analysis results.

Panels A and B depict the simple bivariate association between the Harmonic Power Requirement and Fractal Dimensionality in the real-world datasets. Two-dimensional contours of post-stroke lesions (for ATLAS) and Glioma gross cores (for BRATS) are provided as visual cues of shapes afforded those corresponding scores by HPR and FD indices. Panel C displays additional simulation analyses on sets of 10 circles that demonstrate how the presence of invaginations in the BRATS dataset impacted the association between the two measures. Panel D demonstrates a simple example of the relationship between amount of local complexity present and HPR/FD values.

Table 1
Overview of simulation results.

	HPR intercept	slope	FD intercept	slope
Form	0.82 (0.63, 1.01)	0.01 (-0.01, 0.02)	0.22 (0.17, 0.28)	0.01 (0.001, 0.01)
Random		0.13 (-0.02, 0.28)		-0.23 (-0.27, -0.19)
Regular		-0.03 (-0.18, 0.12)		0.64 (0.60, 0.69)
Amplitude	0.79 (0.73, 0.86)	0.03 (0.01, 0.05)	0.09 (-0.02, 0.19)	0.09 (0.06, 0.12)
Frequency	0.85 (0.79, 0.90)	< 0.01 (-0.001, 0.001)	0.004 (0.003, 0.01)	0.004 (0.003, 0.01)
Rotation	0.86 (0.85, 0.87)	< 0.01, (< 0.01, < 0.01)	0.49 (0.48, 0.50)	< 0.01, (< 0.01, < 0.01)
Percentage	0.65 (0.61, 0.70)	0.002 (0.001, 0.003)	0.13 (0.09, 0.16)	0.01 (0.01, 0.01)

Note. Base group for comparison of form is recursive local complexity. All but the Form models control for form of local complexity (coefficients not shown). Confidence intervals but not significance are reported, as the magnitude and precision of effects are more meaningful here.

sensitive to regular complexity. Coupled with the observation that FD increased as more of the contour was locally complex, while HPR remained comparatively stable, this demonstrates that FD is sensitive to the degree of complexity across the whole contour, while HPR is better suited for detection of the highest frequency present regardless of complexity elsewhere on the contour. Both indices increased as amplitude and frequency increased, however HPR exhibited a wider range at each level of these manipulations. This may be because the HPR captures first global, then local shape information, and so more harmonic power is tied to capturing the global complexity (divergence from an ellipse), consequently reducing sensitivity to local complexity. FD was systematically biased by rotation (periodic relationship between rotation and index can be seen Fig. 2 panel E), likely due to the orientation of the grid used for box counting algorithms. While HPR experienced some bias in rotation in some simulated shapes, this was more random and to a substantially lesser degree.

3.2. Real shapes

Real shape results are summarised in Fig. 3 (panels A and B). The indices were positively correlated in the ATLAS post-stroke lesion contours ($r \approx 0.6$), yet negatively correlated in the BRATS glioma gross cores ($r \approx -0.4$). The most likely explanation for this was that indices diverge substantially in the presence of invaginations, as this was the key shape feature present in BRATS but largely absent from the ATLAS contours. A further contributing element may have been the tendency for FD to be more sensitive to the amount of complexity present, while HPR is more sensitive to the degree (regardless of amount).

3.3. Further exploration of key differences between FD and HPR

A further 60 shapes were simulated. As summarised in Fig. 3 panel C (and supplementary figure 7), these were sets of 10 circles varying in invagination depth (0=shallow to 10=deep), width (0=narrow to 10=wide) and number (0–9), with either no or some local complexity present.

As invagination depth varied, results indicated FD measured primarily local complexity while HPR conflated local and global complexity: t-tests comparing index values with/without local complexity were significant for FD ($t = 4.47$, 95%, $p < 0.01$) but not HPR ($t = 1.89$, $p = 0.12$). Correlation between the two was confounded by two clusters of limited variability in FD (corresponding to no and some local complexity) but a range of values in HPR (corresponding to variations in global shape). As invagination width increased, HPR remained relatively constant while FD varied substantially. While both significantly differentiated with/without local complexity (FD $t = 4.44$, $p < 0.01$; HPR $t = 16.5$, $p < 0.01$), for the width manipulation there is limited variability in HPR (corresponding to no and some local complexity) but a range of values in FD (corresponding to variations in global shape). Both HPR and FD were somewhat sensitive to invagination number, with both increasing as invagination number

increased. While FD still consistently differentiated with/without local complexity ($t = 4.44$, $p < 0.01$), HPR did not ($t = 0.08$, $p = 0.93$), most likely because the difference between zero and one invaginations was detected as a major change in local complexity.

A further point of divergence between the two indices that may have contributed to the observed results is that HPR detects points of highest frequency, while FD averages across the whole contour. This was manifest in results for varying percentage of local complexity, and is demonstrated in Fig. 2 panel F and Fig. 3 panel D. FD smoothly increases as the complexity elsewhere on the contour increases, while there comes a point (specific to each form) where HPR reaches ceiling regardless of additional components of a contour exhibiting local complexity. Taken together, these results indicate that the divergence between FD and HPR when applied to real-world cancer lesion data is likely due to HPR's relative sensitivity to global shape features (invaginations) and comparative insensitivity to the amount (rather than degree) of complexity present.

4. Discussion

This study used a combination of simulated and real contours to clarify the sensitivity, specificity and comparative properties of two indices for measuring local shape complexity in neuroimaging. We found that FD and the proposed HPR index were positively correlated, but diverged in ways that relate to their conceptually distinct operationalisations of local complexity information.

FD was more sensitive to amplitude, frequency, and less biased by global shape features such as the depth of invaginations. However, it was also more vulnerable to bias from rotation, and global shape features such as the width of invaginations. These characteristics arise directly from the use of a grid, where minor shifts in shape orientation and location may cause parts of a contour to become 'counted' or not. This is overcome in HPR, which was comparatively rotation and orientation invariant. However, because HPR is constructed as deviations from an ellipse, global shape forms requiring substantial deformation, such as deep invaginations, require higher frequency harmonics, and so dull sensitivity to features which more closely align with local complexity such as more generalised surface unevenness. These relative strengths and weaknesses align with previous suggestions that Fourier techniques are better suited to elliptical biological forms (Caple et al., 2017; Kuhl and Giardina, 1982), and calls for caution in orientation and grid size selection when applying FD (Walsh and Watterson, 1993). Yet, likely due to the wide range of potential applications of local complexity analysis, there remains an absence of clear guidelines as to precisely how much deviation from an ellipse is tolerable (short of mathematical failure to converge), or how much of a threat rotation poses (short of averaging FD over an arbitrarily large set of orientations). Accordingly, it may be useful to apply both HPR and FD and use divergence in the indices to indicate where bias arising from one or the other may be unduly impacting results.

FD indicated net complexity across the whole contour, because it is

based on a ratio that encompasses the whole contour. HPR provides a distinct perspective by providing a measure of the highest frequency present regardless of complexity elsewhere on the contour, after somewhat accounting for information tied to global features. Accordingly, FD may be most suitable in circumstances where overall complexity is most meaningful (e.g. in differentiating benign from malignant tumors (Wu et al., 2012)), while HPR is better suited for circumstances where peak complexity is of most interest (e.g. in investigating stroke lesions where only part of a neural structure's contour is impacted, as in (Szabo et al., 2009)).

To our knowledge, this is the first systematic benchmarking of FD for neuroimaging applications and suggestion of HPR as an alternative, complimentary metric of local complexity. Accordingly, the scope of this study was limited to a set of selectively manipulated simulated shapes, and two sets of existing manually segmented data, all of which described closed contours. There is substantial scope to apply both FD and HPR in the investigation of open contours (e.g. (Dalitz et al., 2013)'s expansion of Fourier descriptors for open shapes via the convex hull), for applications such as exploring convolution of gyri (e.g. providing a complementary alternative to (Luders et al., 2004)'s global measure of smoothed absolute mean curvature). Similarly, in the interests of generic applicability, analysis was limited to comparison of FD and HPR. This leaves room for further benchmarking against domain-specific measures of shape which relate to local complexity (e.g. compactness and moment-based shape factors used in differentiating malignant from benign cancers as in (Wu et al., 2012)) in future studies. Finally, both FD and HPR are amenable to extension into the third dimension via cube-counting algorithms and Spherical Harmonic Analysis. Given the inherently three-dimensional nature of neuroimaging scans, further benchmarking of their expansion into 3D space would be highly informative.

5. Conclusions

The choice of using one (or both) indices depends on whether the researcher is more interested in measuring the surface complexity of the most irregular part of a contour (in which case HPR is preferable), or an aggregate measure that characterises complexity across the entirety of the contour (in which case FD is preferable). The presence and theoretical importance of global features that may or may not be of interest, such as large invaginations as seen in cancer masses, should also be considered. These results demonstrate there is considerable scope for the HPR to be used in future neuroimaging research.

Competing interests

We have no competing interests.

Disclosure

The authors have reported no conflicts of interest.

Author contributions

EW provided the original idea for the manuscript, conducted all statistical analyses, and managed all aspects of manuscript preparation

and submission. TZ contributed to the design of the study and contributed to writing and editing of the manuscript. NC contributed to the design of the study and contributed to writing and editing of the manuscript.

Funding

EW's position is funded by the National Health and Medical Research Council [grant number 1063907]. NC's Research Fellowship is funded by the Australian Research Council [grant number 120100227].

Acknowledgements

We would like to thank Sook-Lei Liew, Alison Stroud, and the ATLAS team, as well as Spyridon Bakas and the BRATs team for sharing their data.

Appendix A. Supplementary data

Supplementary material related to this article can be found, in the online version, at doi:<https://doi.org/10.1016/j.jneumeth.2019.05.009>.

References

- Bakas, S., Akbari, H., Sotiras, A., Bilello, M., Rozycki, M., Kirby, J.S., Davatzikos, C., 2017. Advancing the cancer genome atlas glioma MRI collections with expert segmentation labels and radiomic features. *Sci. Data* 4, 170117.
- Bonhomme, V., Picq, S., Gaucherel, C., Claude, J., 2014. Momocs: outline analysis using R. *J. Stat. Softw.* 56 (13), 1–24.
- Caple, J., Byrd, J., Stephan, C.N., 2017. Elliptical Fourier analysis: fundamentals, applications, and value for forensic anthropology. *Int. J. Legal Med.* 131 (6), 1675–1690.
- Dalitz, C., Brandt, C., Goebbels, S., Kolanus, D., 2013. Fourier descriptors for broken shapes. *EURASIP J. Adv. Signal Process.* 2013 (1), 161.
- Di Ieva, A., Esteban, F.J., Grizzi, F., Klonowski, W., Martín-Landrove, M., 2015. Fractals in the neurosciences, part II: clinical applications and future perspectives. *Neuroscientist* 21 (1), 30–43.
- Di Ieva, A., Grizzi, F., Jelinek, H., Pellionisz, A.J., Losa, G.A., 2014. Fractals in the neurosciences, part I: general principles and basic neurosciences. *Neuroscientist* 20 (4), 403–417.
- Ferrario, V.F., Sforza, C., Serrao, G., Frattini, T., Del Favero, C., 1994. Shape of the human Corpus callosum: elliptic fourier analysis on midsagittal magnetic resonance scans. *Invest. Radiol.* 29 (7), 677–681.
- Kuhl, F.P., Giardina, C.R., 1982. Elliptic fourier features of a closed contour. *Comput. Graph. Image Process.* 18 (3), 236–258.
- Liew, S.-L., Anglin, J.M., Banks, N.W., Sondag, M., Ito, K.L., Kim, H., Lefebvre, S., 2017. The anatomical tracings of lesions after stroke (ATLAS) dataset-release 1.1. *bioRxiv*, 179614.
- Luders, E., Narr, K.L., Thompson, P.M., Rex, D.E., Jancke, L., Steinmetz, H., Toga, A.W., 2004. Gender differences in cortical complexity. *Nat. Neurosci.* 7 (8), 799.
- Madan, C.R., Kensinger, E.A., 2017. Age-related differences in the structural complexity of subcortical and ventricular structures. *Neurobiol. Aging* 50, 87–95.
- Menze, B.H., Jakab, A., Bauer, S., Kalpathy-Cramer, J., Farahani, K., Kirby, J., Wiest, R., 2015. The multimodal brain tumor image segmentation benchmark (BRATS). *IEEE Trans. Med. Imaging* 34 (10), 1993.
- Szabo, K., Förster, A., Jäger, T., Kern, R., Griebel, M., Hennerici, M.G., Gass, A., 2009. Hippocampal lesion patterns in acute posterior cerebral artery stroke: clinical and MRI findings. *Stroke* 40 (6), 2042–2045.
- Walsh, J., Watterson, J., 1993. Fractal analysis of fracture patterns using the standard box-counting technique: valid and invalid methodologies. *J. Struct. Geol.* 15 (12), 1509–1512.
- Wu, P., Xie, K., Zheng, Y., Wu, C., 2012. Brain Tumors Classification Based on 3D Shape. *Advances in Future Computer and Control Systems*. Springer, pp. 277–283.